AIAA-2003-3424

GRIDFREE SIMULATION OF TURBULENT BOUNDARY LAYERS USING VORCAT*

Peter S Bernard †
University of Maryland
College Park, MD

Pat Collins ‡
Vorcat Inc.
Rockville, MD

Jacob Krispin §
Vorcat Inc.
Rockville, MD

Abstract

The VorCat implementation of the 3D vortex method is described and preliminary applications to boundary layer flow and the flow past a prolate spheroid are discussed. Numerical solutions displaying the non-steady development of the turbulent vorticity field in these settings is presented. Results suggest the viability of the approach in the treatment of difficult, three-dimensional complex turbulent flows that pose significant problems for current turbulence modeling techniques.

Introduction

Large Eddy Simulations (LES) of turbulent flow most often are developed in the context of grid-based numerical schemes in which transport models are used to represent subgrid scale phenomena. Sufficient questions remain about the accuracy and efficiency of such methods that there continues to be interest in the development of alternative formulations of LES. One such approach, with quite different properties than grid-based schemes, is based on the use of gridfree vortex methods where the computational elements are convecting and interacting vortices. Vortex methods give the opportunity to incorporate subgrid scale models with a more direct and natural representation of turublent physics than diffusive transport models. This paper considers one such example of a vortex method appropriate to turbulent flow, namely the VorCat code.

The success of LES depends on capturing the physics of relatively small-scale phenomena as it affects the dynamics of the large scales. As it turns out, phenomena occurring at the subgrid scale are often of great dynamical significance placing large demand on the accuracy of subgrid scale models. Among the important subgrid phenomena are the vortex structure of the near-wall region that is responsible for the Reynolds shear stress [3] and the vortices that stretch and fold taking energy to dissipation scales [13]. The latter can also include backscatter of energy to larger scales, so that simple dissipative models built on scaling properties of the inertial range are not sufficient. Other aspects of the subgrid world include sharp shear layers and other vortical objects that affect the development of the large scale motions.

Since vortex methods are built directly on the use of vortices as computational objects, there should be an intrinsic efficiency to the representation of turbulent flow directly through vortical elements. Besides being a boon to the modeling of small scale vortical phenomena, the need for transport models is eliminated. On the other hand, retrieving the velocity field from vortical objects using the Biot-Savart law, which is a fundamental aspect of vortex methods, is expensive since an N body problem must be solved (each of the vortices in a collection of N will effect the motion of the others).

With the development of fast schemes for evaluating velocities from collections of vortices such as

*VorCat is protected under U.S. Patent No. 6512999
†Professor and CTO of VorCat, Inc.
‡Senior Research Scientist, AIAA Member
§CEO, AIAA Associate Fellow

the Fast Multipole Method (FMM) [6] it becomes possible to reduce the computational labor in implementing the Biot-Savart law to $O(N)$ effort. This means that it becomes practical to perform simulations with millions of elements and thus a reasonable representation of turbulence at the level of a LES. This paper describes recent work in the development of the commercial VorCat code that is specifically designed for the treatment of large scale complex turbulent flows. Some preliminary results for flows containing solid boundaries will be given here, specifically, a zero-pressure gradient boundary layer and the flow around a prolate spheroid at angle of attack. Some recent results for mixing layer flow containing solid particles may be found in [2].

VorCat

In a vortex method the computational elements are vortices, typically either blobs, tubes or sheets, whose dynamics are determined from numerical modeling of the vorticity equation. While blobs are more commonly used in the modeling of viscous diffsion than tubes, they have a tendency to unbounded vorticity growth in situations where resolution becomes lost (e.g., during the natural transition into turbulent flow when sharp flow features arise). Tube-like elements, on the other hand, are stable in such circumstances in the sense that by invoking Kelvin's theorem their circulation remains constant in time and hence bounded. Since the effect of viscosity in turbulent flow is confined to the viscous sublayer adjacent to solid boundaries and to small scale dissipation events throughout the flow, a vortex method LES can be built around the use of tubes without significant handicap and with much to gain in stability and as a natural model for the actual vortices appearing in turbulent flow.

In VorCat, vortices in the form of straight line vortex segments act as the fundamental gridfree element. By moving their end points according to the local fluid velocity, the convection, vortex stretching and reorientation effects in the 3D vorticity equation are modeled. Vortex tubes that stretch beyond a threshold are subdivided. This scheme is largely motivated by computational efficiency, but can, in principle, be improved by tracking smoothly deforming vortices (e.g. using splines) or by taking into account the subtleties of the cross-sectional areas of tubes. Moreover, local violation of the requirement that the vorticity vector be solenoidal is accepted at the end points of filaments, since computational experience to date does not support a need to import techniques that can correct this [8].

In high Reynolds number flows, vortex tubes stretch and fold until they approach the fine scales where viscous dissipation becomes important. Not only is it prohibitively expense to run a vortex method calculation until such scales are populated, but there is no simple means for accurately accommodating viscous diffusion of vortex tubes. These problems can be resolved by noting that there is no need to track the vortex folding process to the viscous scales [5]. Rather, the highly kinked vortex tubes (i.e., hairpins) that are destined to ultimately lose their energy to dissipation after more stretching and folding, can be removed directly. This eliminates primarily local energy since the far field velocity due to hairpins is small.

With the use of the hairpin removal algorithm, a vortex method has the character of a LES, since hairpin removal has the effect of placing a lower bound on the resolved scales. An additional benefit of tubes is that they are the principal dynamical feature of the near-wall region in bounded turbulent flows. Particularly in the form of quasi-streamwise vortices they control the momentum exchange near boundaries that leads to the Reynolds shear stress. Thus, with the use of a tube method, it becomes a relatively simple matter to examine and insure that there is a proper coverage of vortex elements in the wall region.

Vortex sheets

Solid boundaries pose a number of problems to vortex methods since the largely two-dimensional vorticity layers covering them are not easily represented through blob or tube-like elements. As illustrated in Fig. 1 showing the mean vorticity in a DNS of channel flow [7], the vorticity undergoes large gradients in the viscous sublayer of turbulent flow that must be well represented if an accurate estimate is to be made of the flux of vorticity into the flow. In VorCat a thin unstructured mesh of triangular prisms is used to cover the viscous sublayer next to solid walls, as seen in Fig. 1. The sheets are stacked normal to the surface several layers deep, with a half-thickness sheet adjacent to the boundary, and extend to approximately $y^+ = 30$. The vorticity that gets to the top surface sheets is turned into vortex tubes in imitation of the process by which new vortices appear in turbulent flow during ejection events in the wall layer. It should also be noted that the use of triangular mesh is compatible with typical engineering design studies that provide information about the

shape of solid bodies in the form of triangularizations of the surface. Thus the boundary treatment in VorCat is relatively simple to enact.

The 3D vorticity equation

$$\frac{\partial \mathbf{\Omega}}{\partial t} + (\nabla \mathbf{\Omega})\mathbf{u} = (\nabla \mathbf{u})\mathbf{\Omega} \ + \frac{1}{R_e}\nabla^2 \mathbf{\Omega}, \qquad (1)$$

where $\mathbf{u}$ is the velocity, $\mathbf{\Omega}$ is the vorticity and R_e is the Reynolds number is used to update the vorticity distribution in the sheets. The convection and stretching terms are approximated with a finite volume scheme where the convection term is upwinded and first order accurate, and the stretching term is second order. Computation of the Laplacian is split into normal and tangential parts. The normal part is approximated with a second order finite difference formula and the tangential part is computed by differentiating a least squares polynomial approximation.

Velocity field

In a vortex method the velocity field is recovered from the vorticity field via

$$\mathbf{u}(\mathbf{x}, t) = \int_{\Re^3} K(\mathbf{x} - \mathbf{x}')\mathbf{\Omega}(\mathbf{x}', t)d\mathbf{x}' + \mathbf{u}_p(\mathbf{x}, t), \quad (2)$$

where

$$K(x, y, z) = -\frac{1}{4\pi \mid \mathbf{x} \mid^3} \begin{pmatrix} 0 & -z & y \\ z & 0 & -x \\ -y & x & 0 \end{pmatrix}, \quad (3)$$

is the Biot-Savart kernel and $\mathbf{u}_p$ is a potential flow added to enforce the non-penetration boundary condition at solid surfaces. Following standard practice [5, 8], that part of the integral in (2) due to the ith vortex is approximated via

$$\int_{\Re^3} K(\mathbf{x}-\mathbf{x}')\mathbf{\Omega}(\mathbf{x}', t)d\mathbf{x}' \approx -\frac{\Gamma_i}{4\pi}\frac{\mathbf{r}_i \times \mathbf{s}_i}{\mid \mathbf{r}_i \mid^3}\, \phi(r/\sigma) \quad (4)$$

where

$$\phi(r) = 1 - \left(1 - \frac{3}{2}r^3\right) e^{-r^3}$$

is a high-order smoothing function, Γ_i is the circulation, $\mathbf{r}_i = \mathbf{x} - \mathbf{x}_i$, $\mathbf{x}_i$ is the tube center, $\mathbf{s}_i$ is an axial vector along the length of the tube and σ is a smoothing parameter.

The velocity due to the triangular-prism sheets is determined by integrating the exact formula in (2) over the triangular area assuming a piecewise linear vorticity field and neglecting variations in the wall-normal direction. After integration the singularity in $K(\mathbf{x}-\mathbf{x}_i)$ is eliminated except at the edges of the triangles where a finite velocity obtained as the end result of a cancellation of the contribution from the adjacent triangle. These special cases are handled in the code by forcing analytic cancellation.

The potential flow necessary to ensure non-penetration is derived from a collection of source panels covering the same unstructured triangular surface mesh as used in computing the sheet vorticity field. A piecewise linear distribution of the source strength field, q, is assumed. q is determined from numerical solution of the defining equation

$$\frac{1}{4\pi}\int_S \frac{q(\mathbf{n}\cdot\mathbf{r})}{r^3} dS' = -\mathbf{n}\cdot\mathbf{u}_\mathbf{v} \qquad (5)$$

where $\mathbf{r} = \mathbf{x} - \mathbf{x}'$. The left-hand side is the surface normal velocity induced on the surface point $\mathbf{x}$ by q and the right-hand side is the opposite of the surface normal velocity induced by the vortex elements. By enforcing the boundary condition at the node points of the triangularized surface, a linear system of equations for nodal point source strengths results, namely,

$$A_{ij}q_j = -\mathbf{n}\cdot\mathbf{u}_{\mathbf{v_i}} \qquad (6)$$

where each element of A_{ij} is the normal velocity induced at surface node point i by a piecewise linear source distribution with unit strength at node point j and zero elsewhere. This equation is solved using the GMRES iterative scheme [9]. The evaluation of $\mathbf{u}_p$ from the source panels involves integrals identical to those appearing from the Biot-Savart law, so the same integral evaluations can be used for both purposes.

Vorticity in the half-thickness vortex sheets touching solid surfaces is determined via finite difference approximation to velocity derivatives assuming the no-slip boundary condition. The vorticity in the wall sheets does not contribute to the velocity elsewhere in the flow since it is imagined to be matched with vorticity of opposite sign residing in a half-thickness image vortex sheets at the boundary surface. In other words, a wall sheet and its image induce a velocity tangential to the wall in the region between them: one which balances the velocity due to all other sheets and vortices. Elsewhere, these vortices do not contribute to the velocity because of cancellation of their opposite signed vorticity.

Fast Multipole method

VorCat relies on an adaptive, parallel implementation of the FMM [6, 11]. In this the flow domain

is successively partitioned into nested cubic boxes with the goal of placing a predetermined number of vortices into each box. Regions with a high concentration of vortices are covered by many small boxes, whereas, regions with few vortices have a small number of large boxes.

The FMM works by combining the vector potential induced by vortices in the root boxes into truncated expansions in spherical harmonics about the centers of the boxes. The expansions are combined into expansions over parent boxes at higher levels in the tree. Expansions at the highest level are then shifted down a separate tree of field points formed from boxes containing the points where the velocity needs to be evaluated. The cumulative effect of many vortices is thus brought down to the evaluation of a single expansion at the root level of the field tree. The smallest allowable box is limited by the parameter σ that controls the region where smoothing of the Biot-Savart kernel occurs. Since $\phi = 1$ for $r > 2.34$ the smallest allowable box in the FMM must have side 2.34σ. This requirement can lead to less than optimal distribution of vortices. To maintain the speed of the code a middleman approach is used where the velocities from vortices in the local calculation are computed at the nodes of nearby boxes and 3D linear interpolation used to get the velocities at the vortex locations. In view of the smoothness of the local velocity, this procedure does not lead to any significant loss of accuracy.

Considerable effort at parallelizing the FMM algorithm has been expended and more is planned for the future. Figure 2 shows that excellent scalability is achieved up to 16 processors. Beyond this point the increasingly difficult task of load balancing reduces efficiency. Several steps for better distributing work among large number of processors are currently being implemented. In the meantime, the figure shows that a velocity computation involving 4 million vortices can be accomplished in under a minute with 64 processors. This is sufficient to accomplish large scale computations in a reasonable time frame.

Results

As part of an ongoing effort at benchmarking the capabilities of VorCat, the code has been applied to a number of configurations that can help to establish its effectiveness in modeling turbulent flows. Here, some prelimanary results are given for the prediction of turbulent flow in a zero-pressure gradient boundary layer and past a 6:1 prolate spheroid at 30° angle of attack. This work is preliminary in the sense that it is based on the use of relatively coarse reresentations of the viscous sub-layer in terms of triangularizations. Better resolved models of these flows are currently under investigation using a new version of the code that removes previous memory limitations.

Boundary layer

The study of the zero-pressure gradient boundary layer has been ongoing effort at VorCat in view of the substantial amount that is known about it from physical experiments and numerical simulations. Figure 3 shows the computational domain, marked in red, with periodic images of the flat plate to either side. The use of image vortex systems in satisfying periodidc boundary conditions is a necesary consequence of the use of the Biot-Savart law. By taking advantage of the translation properties of the FMM solver, the cost of the image vortices can be reduced substantially over the cost of the vortices in the main test section. As seen in the figure, 16 images of the main section are used. This means that for runs with 4 million vortices in the main section, the influence of approximately 68 million vortices is taken into account.

The zero-pressure-gradient turbulent boundary layer is solved from an upstream laminar flow past a trip causing transition to turbulence, much as it is commonly done in physical experiments. Special care in implementing upstream and downstream boundary conditions is necessary. For example, in a vortex method the vorticity that would naturally exist downstream of any arbitrary end point to the plate affects motion upstream [1], and this needs to be taken into account in the downstream boundary conditions.

Figures 4 and 5 show the vortex elements in a boundary layer calculation as viewed from above and side, respectively. The flow is tripped by a bump placed at x=0.1 with height 0.003. The plate used in the simulation has a total length of 2 and the Reynolds number $Re_x = U_\infty x/\nu = 400,000$ at the end of the plate. Upstream of the trip, the vortices are purely spanwise and the flow is laminar. Immediately downstream of the bump the flow remains laminar for a short distance, but soon transitions into a highly perturbed state. This behavior is reminiscent of the physical transition process in which 2D Tollmein-Schlichting waves first appear, followed by a focusing of their spanwise vorticity, that subsequently undergoes instability causing the appearance of streamwise vorticity and finally turbulence.

A close-up view of the vortex elements in the latter part of the transition region is shown in Fig. 6. Spanwise vorticity originating at the surface has diffused outward and turned into spanwise vortex elements. These fill up the laminar and transitional flow regions. Subsequently, many vortices reorient into the streamwise direction in association with regions of faster and slower streamwise flow, i.e., the beginnings of the streaky structure that characterizes turbulent boundary layers and underlies the fully turbulent regions of the simulation. With the appearance of the streamwise vorticity the flow becomes turbulent. It is also the case that the vortices combine in groups to form structures of a larger scale than any one vortex, as is evident from Figs. 4 and 5.

Viewed from the side in Fig. 5, the boundary layer thickens quickly after transition and continues to grow downstream. The bulges visible at the outer surface are characteristic of physical boundary layer visualizations [3]. Like the physical case, they suggest the presence of incursions of the outer flow deep into the boundary layer. The vortices indicate the presence of a relatively sharp boundary between turbulence and the potential flow, as is also seen in experiments. Further downstream the flow develops many structural features in the form of coherent vortices. Their appearance has much in common with similar objects seen in smoke visualizations of the turbulent boundary layer

Within the computed boundary layer are many strong streamwise vortices of plus and minus rotation. These drive momentum to and from the wall creating a substantial negative Reynolds shear stress in the simulation. A preliminary calculation of the average mean velocity at $x = 0.8$ corresponding to $Re_x = 160,000$ taken from a small set of flow realizations is given in Fig. 7. $\overline{U}(y)$ is plotted vs. the standard log law result $\overline{U}^+ = (1/.41)\log y^+ + 5$, the near-wall relation $\overline{U}^+ = y^+$, and a DNS prediction [10] at $R_\theta = 670$. It is evident that the physical trend is well duplicated. Complete sets of turbulence statistics will be obtained for new high-resolution simulations.

Prolate spheroid

The flow past a 6:1 prolate spheroid under a variety of conditions has been the object of considerable attention in physical experiments [4, 14] and thus provides a convenient venue with which to examine the effectiveness of our vortex method in predicting high Reynolds number flows. VorCat has recently been applied to the case of a 30° angle of attack with Reynolds numbers based on free stream velocity and axial length of 150,000 and 1.6 million. The case with 4.2 million corresponds to experiments and some results on this flow are just beginning to be computed. In this work, the prolate spheroid surface is covered with 9936 triangles, 10 layers of vortex sheets are used and by the end of a calculation to time 1.56 there are approximately 2.5 million tubes.

Figs. 8 - 10 show views from the side, top and back, respectively of the approximately strongest 20% of the vortices at time 1.56. There is also considerable vorticity (not depicted) in the vortex sheets adjacent to the surface. Flow separation occurs along the leeward side over a region that is perhaps narrower than that seen in experiments at higher Reynolds number. Since experiments use stings in the back and boundary layer trips near the front, some caution must be exercised in making strict comparisons (i.e. there can be significant sensitivty to Reynolds number). This is currently under investigation while finer resolution calculations are being carried out. The size of the separated region is suggested in Figs. 11 and 12 showing the velocity u at the second sheet level and the pressure p on the surface calculated using an integral formulation [12]. Evidently, these properties are sufficiently good to give the force predictions in Fig. 13 that agree well with a range of experiments. For example, the total (viscous + pressure) force in the y direction is seen to fluctuate around 0.03 which is in the range (0.027 - 0.030) seen in experiments at this angle of attack [4, 14].

Conclusion

The vortex method for turbulent flow simulation described herein has made a promising start toward achieving the capability of efficiently modeling complex, high Reynolds number turbulent flows. Reasonable force and pressure predictions have been made; flow and wake structure developing in the boundary layer and the prolate spheroid show many physical features. Future work will have enhanced sublayer resolution and exhaustive comparisons with high Reynolds number experiments will be carried out.

Acknowledgements

This research has been supported through an ATP/NIST award to VorCat, Inc. Computer time

is provided in part by NCSA.

References

[1] Bernard, P.S. (1995) "A deterministic vortex sheet method for boundary layer flow," *J. Comp. Phys.*, **117**, pp. 132 - 145.

[2] Bernard, P. S., Potts, M. and Krispin, J. (2003) "Studies of turbulent mixing using the VorCat implementation of the 3D vortex method," AIAA Paper No. AIAA-2003-3599.

[3] Bernard, P.S. and Wallace, J.M. (2002) *Turbulent Flow: Analysis, Measurement and Prediction*, John Wiley & Sons.

[4] Chesnakas, C. J., and Simpson, R. L. (1994) "Full three-dimensional measurements of the cross-flow separation region of a 6:1 prolate spheroid," Experiments in Fluids, Vol. 17, p. 68-74.

[5] Chorin, A. J. (1993), "Hairpin removal in vortex interactions II," *J. Comput. Phys.*, **107**, p. 1-9.

[6] Greengard, L. and Rokhlin, V. (1987), "A fast algorithm for particle simulations," J. Comput. Phys., Vol. 73, p. 325-348.

[7] Moser, R,D., Kim, J. and Mansour, N. N. (1999) "DNS of Turbulent Channel Flow up to $R_\tau = 590$," *Phys. Fluids* **11**, 943 - 945.

[8] Puckett, E. G. (1993), "Vortex methods: an introduction and survey of selected research topics," in *Incompressible Computational Fluid Dynamics: Trends and Advances*, M. D. Gunzburger and R. A. Nicolaides, ed., Cambridge University Press, p. 335-407.

[9] Saad, Y. and Schultz, M. H. (1986) "GMRES: A generalized minimal residual algorithm for solving nonsymmeric linear systems," *SIAM J. Sci. Stat. Comput.* **7**, 856 - 869.

[10] Spalart, P.R. (1988) "Direct simulation of a turbulent boundary layer up to $Re_\theta = 1410$," *J. Fluid Mech.* **187**, 61 - 98.

[11] Strickland, J. H. and Baty, R. S. (1993), "A three dimensional fast solver for arbitrary vorton distributions," *Technical Report SAND93-1641*, Sandia National Laboratories.

[12] Uhlman Jr., J. S. (1992), "An integral equation formulation of the equations of motion of an incompressible fluid," NUWC-NPT Technical Report 10,086, Naval Undersea Warfare Center Division, Newport, Rhode Island.

[13] Vincent, A. and Meneguzzi, M. (1991) "The spatial structure and statistical properties of homogeneous turbulence," *J. Fluid Mech.* **225**, 1 - 20.

[14] Wetzel, T. G., Simpson, R. L. and Chesnakas, C. J. (1998), "Measurement of three- dimensional crossflow separation," AIAA Journal, Vol. 36, p. 557-564.

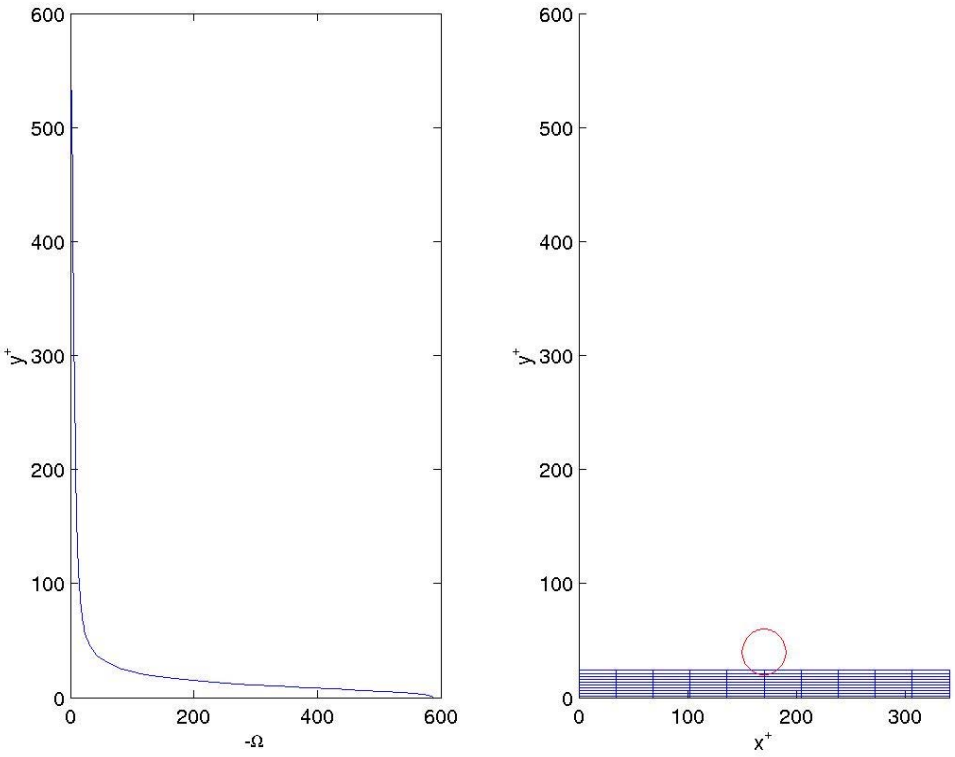

Figure 1: Relationship between the mean vorticity in turbulent flow [7] and the sublayer mesh.

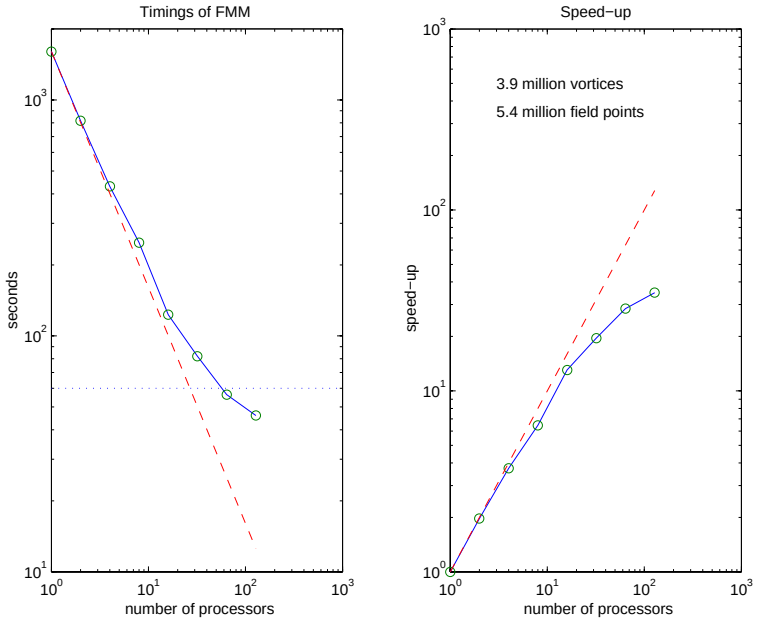

Figure 2: Timings and speed-up of FMM.

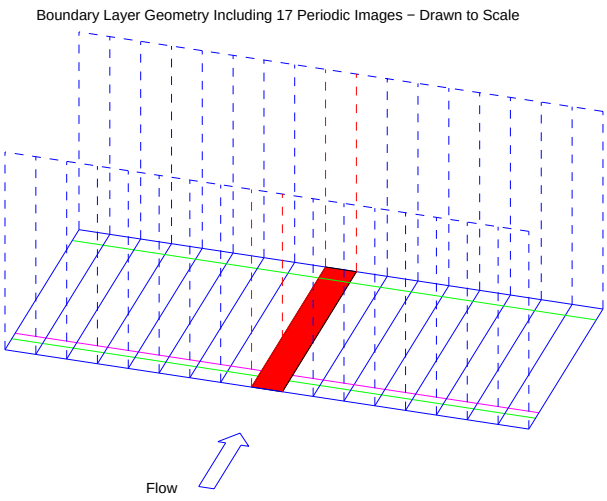

Figure 3: Geometry for boundary layer calculation.

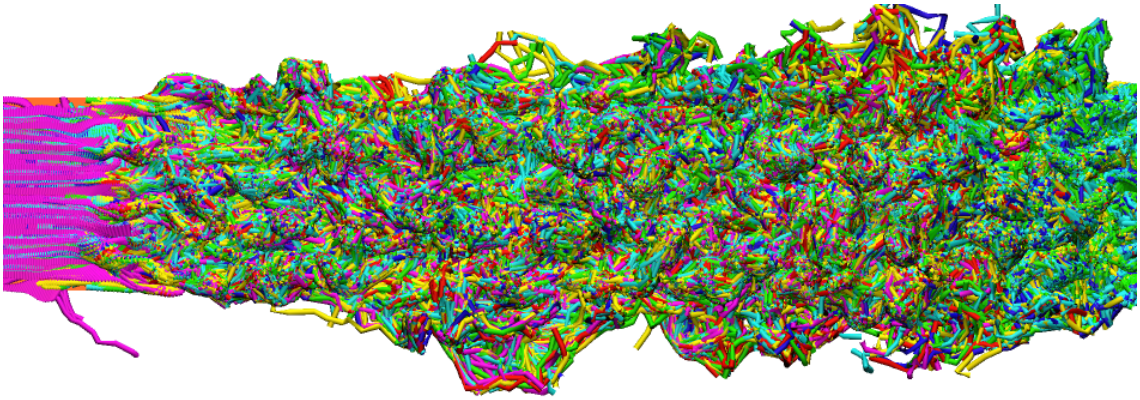

Figure 4: View from above of vortex tubes in a zero-pressure gradient boundary layer.

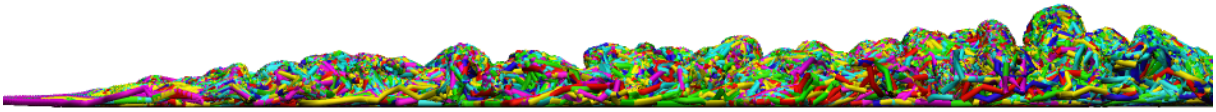

Figure 5: Side view of vortex tubes in a zero-pressure gradient boundary layer.

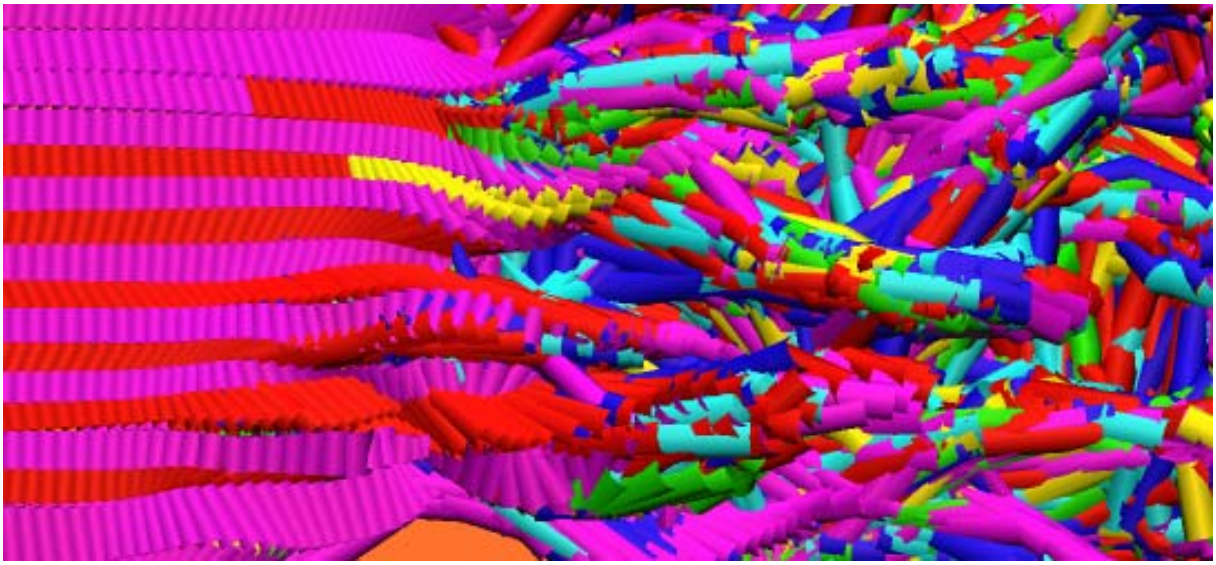

Figure 6: Detail of Fig. 1 in late transition showing the reorientation of spanwise vortices and the development of turbulence structure.

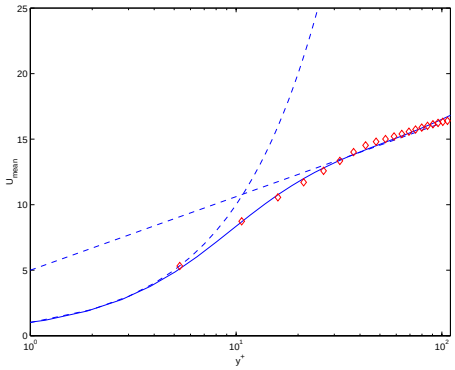

Figure 7: $\overline{U}$ at $x = 0.8$. $- - -$, DNS [10]; $\diamond$, vortex method.

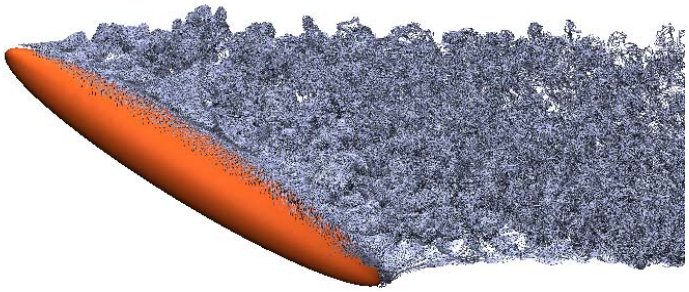

Figure 8: Side view of prolate spheroid showing top 20% of vortices.

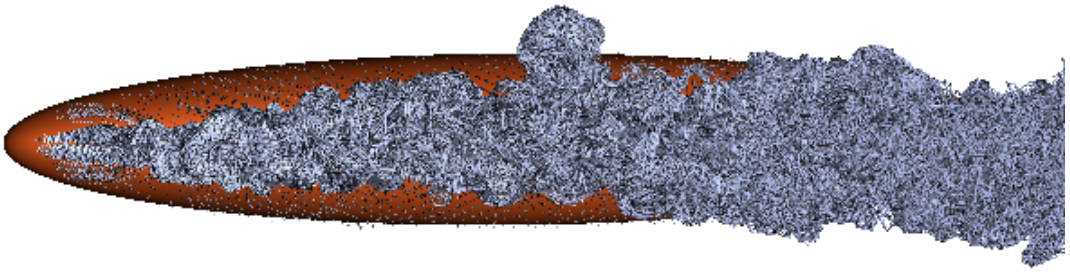

Figure 9: Top view of prolate spheroid showing top 20% of vortices.

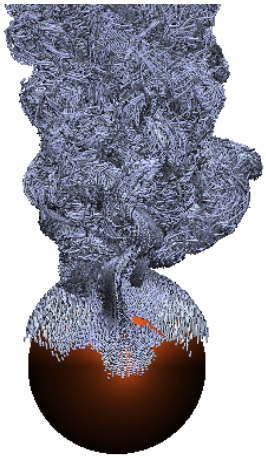

Figure 10: Rear view of prolate spheroid showing top 20% of vortices.

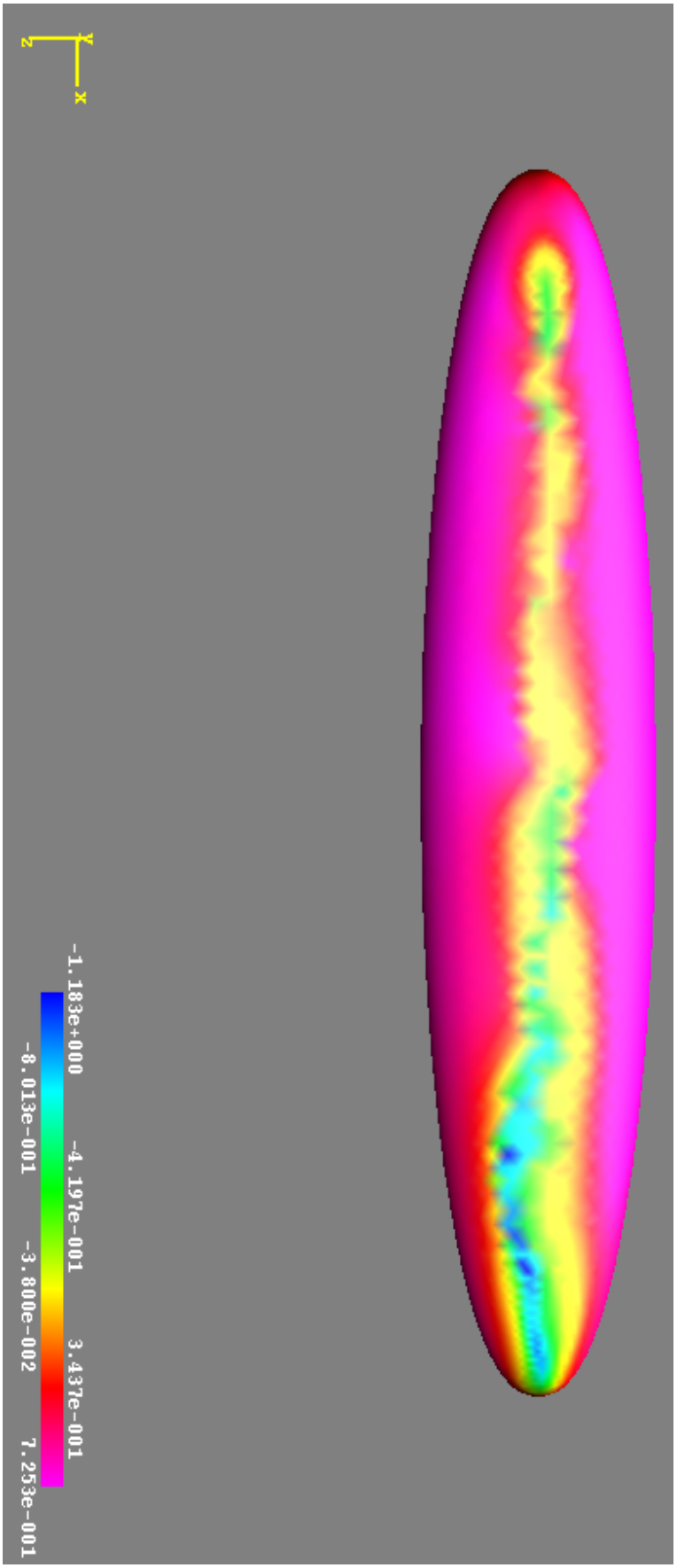

Figure 11: Axial velocity just above leeward surface.

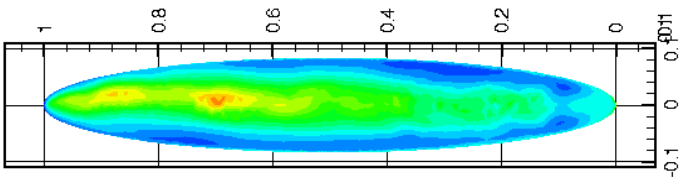

Figure 12: Pressure on leeward surface.

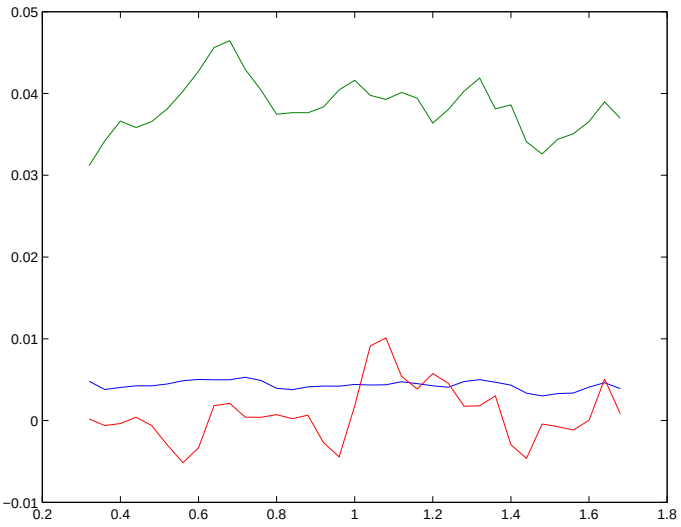

Figure 13: Force coefficients in x (blue); y (green); z (red), directions.